Available online at www.sciencedirect.com

ScienceDirect

IFAC Papers Online CONFERENCE PAPER ARCHIVE

IFAC PapersOnLine 51-2 (2018) 463–468

Towards Port-Hamiltonian Modeling of Multi-Carrier Energy Systems: A Case Study for a Coupled Electricity and Gas Distribution System

Felix Strehle * **Martin Pfeifer** * **Lukas Kölsch** *
Charlotte Degünther ** **Johannes Ruf** ** **Lisa Andresen** ***
Sören Hohmann *

* *Karlsruhe Institute of Technology (KIT), Kaiserstraße 12, 76131 Karlsruhe, Germany (e-mail: {felix.strehle,martin.pfeifer,lukas.koelsch,soeren.hohmann}@kit.edu).*
** *DVGW Research Centre at Engler-Bunte-Institute (EBI) of Karlsruhe Institute of Technology (KIT), Engler-Bunte-Ring 3, 76131 Karlsruhe, Germany, (e-mail: {deguenther,ruf}@dvgw-ebi.de)*
*** *Hamburg University of Technology, Am Schwarzenberg-Campus 1, 21073 Hamburg, Germany (e-mail: andresen@tuhh.de)*

Abstract:
Multi-carrier energy systems have been identified as a major concept for future energy supply. For their operation, model-based control methods are necessary whose design requires modular, multi-physical control-oriented models. In literature, there exists no control design model which combines the variables of the networks and system dynamics that go beyond ideal storage elements. Port-Hamiltonian systems represent a promising approach for the scalable modeling and control of multi-carrier energy systems. In this publication we present a case study which illustrates the port-Hamiltonian modeling of an exemplary coupled electricity and gas distribution system. Simulations indicate the plausibility of the presented model.

Keywords: Modeling, Multi-Carrier Energy Systems, Port-Hamiltonian Systems, Bond Graphs

1. INTRODUCTION

Multi-carrier energy distribution systems (MEDSs) consist of distribution networks for different energy carriers (e.g. electricity, gas, district heat) which are coupled by energy converting devices. Model-based control methods enable a safe, reliable, and efficient operation of MEDSs (Rehtanz, 2014). Multi-physical control-oriented models of MEDSs represent the starting point for the design of such control methods. Due to the complexity of MEDSs, modularity and scalability are key requirements for the models. A MEDS can be subdivided into three basic types of components: (a) subsystems for the generation, conversion, storage, and consumption of energy; (b) networks for the distribution of energy; (c) interfaces for controllable and uncontrollable interaction with the system environment. Following from these components, a MEDS model has to take account of variables which are related to (a) the dynamics of the MEDS; (b) the state of the network, e.g. voltages and currents in the electrical network, or pressures and volume flows in the gas network; (c) the controllable or uncontrollable interaction with the system environment.

Mancarella (2014) provides an overview and discussion of different models for multi-carrier energy systems. The most widespread approach is the power flow-based energy hub concept (Geidl and Andersson, 2005) and extensions thereof (Schulze and Del Granado, 2010). Following an input-output paradigm, energy hubs are capable of modeling conversion and storage of energy. However, the networks are not part of the concept. Arnold et al. (2009) extend the energy hub concept by networks. However, system dynamics are still limited to storage elements which impedes the integration of more complex dynamic subsystems such as second or third order generator models (Dörfler and Bullo, 2012). Besides energy hubs, there is a number of simulation-oriented approaches for modeling multi-carrier energy systems. In their most general form these approaches lead to differential-algebraic equations (DAEs) or partial DAEs (Jansen and Tischendorf, 2014) that are not applicable for control design. Martinez-Mares and Fuerte-Esquivel (2012) and Sirvent et al. (2017) propose simplified steady state models for coupled electricity and gas transmission systems. The models contain the network variables; system dynamics are not incorporated. de Durana et al. (2014) developed an agent-based multi-carrier energy system model, which incorporates the network variables and system dynamics induced by storage systems. However, the model does not consider the constitutive relations of the gas network. In conclusion, to the best of the authors' knowledge, there exists no control-oriented model of MEDSs which combines the network variables, their constitutive relations, and system dynamics that go beyond storage elements.

10.1016/j.ifacol.2018.03.078

Due to their multi-physical and modular nature, port-Hamiltonian systems (PHSs) represent a promising approach for the modeling and control of MEDSs with great potential for the scalability of methods. There have been studies addressing the modeling of electrical power systems with PHSs (Fiaz et al., 2013). However, this is the first study which investigates the modeling of MEDSs with PHSs. The investigation is based on a case study in which an exemplary 20 kV electrical distribution system coupled with a 3 bar (gauge pressure) gas distribution system is modeled. The approach can serve as a blueprint for the modeling of comparable MEDSs. The contributions of this publication are as follows: (a) formulation of the constitutive relations of the network variables for an electrical distribution network and a gas distribution network in the generalized bond graph (GBG) framework; (b) integration of the network models into a PHS model of an exemplary MEDS, which includes a wind turbine, a power-to-gas (P2G) unit, a battery system, and a gas storage; (c) simulation and plausibility check of the MEDS model on the basis of real measurement data and data from state-of-the-art simulation software.

2. BASIC CONCEPT

PHSs are based on the idea of port-based modeling, which focuses on the conservation of energy as a fundamental physical property. A key aspect of the PHS framework is the mathematical formalization of network interconnection structures as *Dirac structure* which can be identified with the *generalized junction structure* of a GBG. It comprises elements of type 0-/1-junction, transformer, and gyrator. Depending on the representation of their underlying Dirac structure, PHSs can either be represented in an explicit form such as the *input-state-output* form

$$\dot{\boldsymbol{x}} = (\boldsymbol{J}(\boldsymbol{x}) - \boldsymbol{R}(\boldsymbol{x}))\,\frac{\partial H}{\partial \boldsymbol{x}}(\boldsymbol{x}(t)) + \boldsymbol{g}(\boldsymbol{x})\boldsymbol{u} + \boldsymbol{k}(\boldsymbol{x})\boldsymbol{d} \qquad (1)$$

(with $\boldsymbol{J}(\boldsymbol{x}) = -\boldsymbol{J}^{\mathsf{T}}(\boldsymbol{x})$, $\boldsymbol{R}(\boldsymbol{x}) = \boldsymbol{R}^{\mathsf{T}}(\boldsymbol{x}) \geq \boldsymbol{0}$, $H(\boldsymbol{x})$ being the Hamiltonian of the system, $\boldsymbol{u}$ being the vector of controlled interaction, and $\boldsymbol{d}$ being the vector of uncontrolled interaction) or by an implicit representation

$$\boldsymbol{F}_1\,\dot{\boldsymbol{x}}(t) = \boldsymbol{E}_1\,\frac{\partial H}{\partial \boldsymbol{x}}(\boldsymbol{x}(t)) + \boldsymbol{F}_2\,\boldsymbol{f}_2(t) + \boldsymbol{E}_2\,\boldsymbol{e}_2(t) \qquad (2)$$

with $(\dot{\boldsymbol{x}}, \partial H(\boldsymbol{x})/\partial \boldsymbol{x}, \boldsymbol{f}_2, \boldsymbol{e}_2)$ satisfying the constitutive relations of the energy storage, resistive, control, and interaction elements (Duindam et al., 2009, pp. 85–89). Equation (2) results from a Dirac structure in *kernel representation*

$$\underbrace{[\boldsymbol{F}_1 \mid \boldsymbol{F}_2]}_{\boldsymbol{F}} \begin{bmatrix} -\dot{\boldsymbol{x}} \\ \boldsymbol{f}_2 \end{bmatrix} + \underbrace{[\boldsymbol{E}_1 \mid \boldsymbol{E}_2]}_{\boldsymbol{E}} \begin{bmatrix} \partial H(\boldsymbol{x})/\partial \boldsymbol{x} \\ \boldsymbol{e}_2 \end{bmatrix} = \boldsymbol{0} \qquad (3)$$

satisfying

$$\operatorname{rank}[\,\boldsymbol{F} \mid \boldsymbol{E}\,] = n, \qquad \boldsymbol{F}, \boldsymbol{E} \in \mathbb{R}^{n\times n}, \qquad (4)$$

$$\boldsymbol{E}\boldsymbol{F}^{\mathsf{T}} + \boldsymbol{F}\boldsymbol{E}^{\mathsf{T}} = \boldsymbol{0}. \qquad (5)$$

PHSs provide a promising approach for systematic modeling of MEDSs, since their structural properties can be related to the inherent characteristics of MEDSs:

Multi-physical nature PHSs enable the handling of MEDSs within one single framework. Moreover, the Hamiltonian $H(\boldsymbol{x})$ provides an important information for the operation of MEDSs as it represents the total stored energy in the system.

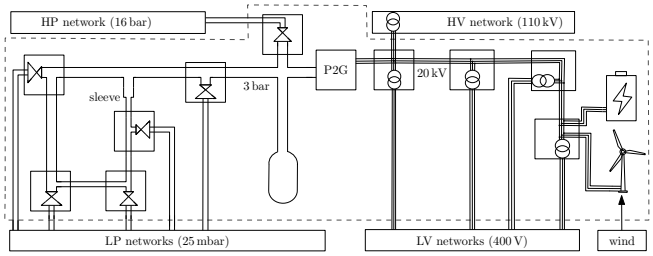

Fig. 1. Schematic of the exemplary system

Modularity PHSs provide a separation of system topology and physical characteristics of components. Moreover, the power-conserving interconnection of PHSs leads to a PHS as well (Duindam et al., 2009, pp. 99–107), which offers great potential for the development of scalable control methods for MEDSs.

3. CASE STUDY

In this section, we present the modeling of a coupled electricity and gas distribution system which is based on a real energy system. The model aims at an application to energy management control and MEDS monitoring and thus incorporates dynamic processes with time constants $T \geq 1$ s. The modeling procedure is as follows: (i) definition of subsystems and abstraction of the MEDS as a directed graph, (ii) modeling of the subsystems, (iii) composition of the entire system model by extracting a Dirac structure from the generalized junction structure of the overall GBG.

As shown in Fig. 1, the electrical system is given by a three-phase 20 kV medium voltage (MV) network with four transformer substations. At the first substation, the network is connected to a 110 kV high voltage (HV) network. Each substation is connected to a subordinate 400 V low voltage (LV) network. The last substation is connected to a wind turbine and a battery system. The gas system consists of a meshed 3 bar infrastructure (gauge pressure) with six gas pressure regulating stations. The first pressure regulating station is connected to a 16 bar high pressure (HP) gas transmission system. Between the first and second pressure regulating station, there is a branch where a gas storage is connected. The regulating stations supply the customers at 25 mbar low pressure (LP) level. Note that along the mesh there are pipes with different diameters which may be connected by a sleeve. The electricity and gas distribution systems are coupled via a P2G unit. In Fig. 1, the system boundary is depicted by a dashed line. As can be seen, superordinate and subordinate networks as well as the ambient atmosphere are interpreted as part of the system environment.

3.1 Abstraction as Directed Graph

According to Hohmann et al. (2017), a MEDS can be abstracted as a directed graph. For the example system, the abstraction is depicted in Fig. 2. Transformer substations, pressure regulating stations, branch points, sleeves, and subsystems for the generation, conversion or storage of energy are modeled as vertices. The superordinate and subordinate networks are modeled by a single super source

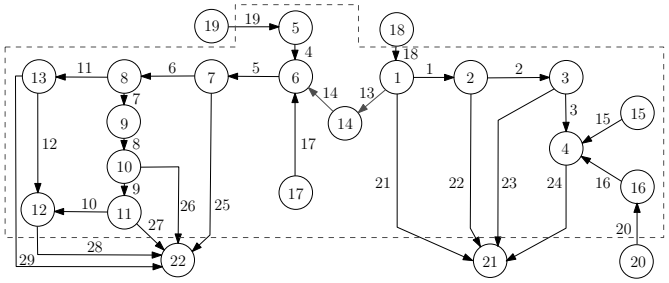

Fig. 2. Directed graph of the exemplary system

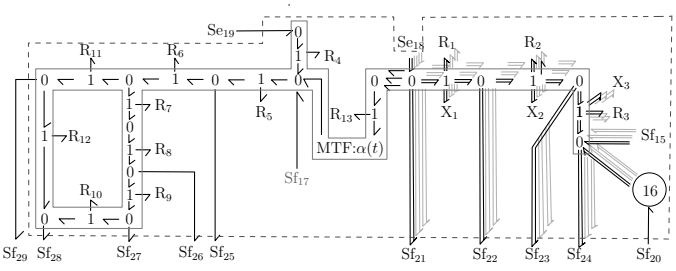

Fig. 3. GBG of the exemplary system

vertex and a super sink vertex for each energy carrier. Moreover, the inflow of wind power is also represented by a source vertex. We assume the vertices $\mathcal{V}_\mathrm{e} = \{1, 2, 3, 4\}$ to represent transformer substations, the vertices $\mathcal{V}_\mathrm{g} = \{5, \dots, 13\}$ to represent vertices of the gas network, the vertex $\mathcal{V}_\mathrm{c} = \{14\}$ to represent the P2G unit, the vertices $\mathcal{V}_\mathrm{d} = \{15, 16, 17\}$ to represent subsystems for the generation or storage of energy, the vertices $\mathcal{V}_\mathrm{s} = \{18, 19, 20\}$ to represent source vertices, and the vertices $\mathcal{V}_\mathrm{t} = \{21, 22\}$ to represent sink vertices. Lines, pipes, and connections to subsystems, sources or sinks are modeled by edges. We assume the edges $\mathcal{E}_\mathrm{e} = \{1, 2, 3\}$ to represent lines, the edges $\mathcal{E}_\mathrm{g} = \{4, \dots, 12\}$ to represent pipes, the edges $\mathcal{E}_\mathrm{c} = \{13, 14\}$ to represent the P2G input and output, the edges $\mathcal{E}_\mathrm{d} = \{15, 16, 17\}$ to represent connections to subsystems, the edges $\mathcal{E}_\mathrm{s} = \{18, 19, 20\}$ to represent connections to source vertices, and the edges $\mathcal{E}_\mathrm{t} = \{21, \dots, 29\}$ to represent connections to sink vertices. Altogether, a graph $G = (\mathcal{V}, \mathcal{E})$ is obtained, where $\mathcal{V} = \cup_{j\in\Lambda}\mathcal{V}_k$ and $\mathcal{E} = \cup_{j\in\Lambda}\mathcal{E}_k$ with $\Lambda = \{\mathrm{e}, \mathrm{g}, \mathrm{c}, \mathrm{d}, \mathrm{s}, \mathrm{t}\}$. The incidence matrix of the graph is of the following structure

$$\boldsymbol{B} = \begin{bmatrix} \boldsymbol{B}_\mathrm{e} & \boldsymbol{0}_{4\times9} & \boldsymbol{B}_{\mathrm{c,e}} & \boldsymbol{B}_{\mathrm{d,e}} & \boldsymbol{B}_{\mathrm{s,e}} & \boldsymbol{B}_{\mathrm{t,e}} \\ \boldsymbol{0}_{8\times3} & \boldsymbol{B}_\mathrm{g} & \boldsymbol{B}_{\mathrm{c,g}} & \boldsymbol{B}_{\mathrm{d,g}} & \boldsymbol{B}_{\mathrm{s,g}} & \boldsymbol{B}_{\mathrm{t,g}} \\ \boldsymbol{0}_{1\times3} & \boldsymbol{0}_{1\times9} & \boldsymbol{B}_\mathrm{c} & \boldsymbol{0}_{1\times3} & \boldsymbol{0}_{1\times3} & \boldsymbol{0}_{1\times9} \\ \boldsymbol{0}_{3\times3} & \boldsymbol{0}_{3\times9} & \boldsymbol{0}_{3\times2} & -\boldsymbol{I}_{3\times3} & \boldsymbol{B}_{\mathrm{s,d}} & \boldsymbol{0}_{3\times9} \\ \boldsymbol{0}_{3\times3} & \boldsymbol{0}_{3\times9} & \boldsymbol{0}_{3\times2} & \boldsymbol{0}_{3\times3} & -\boldsymbol{I}_{3\times3} & \boldsymbol{0}_{3\times9} \\ \boldsymbol{0}_{2\times3} & \boldsymbol{0}_{2\times9} & \boldsymbol{0}_{2\times2} & \boldsymbol{0}_{2\times3} & \boldsymbol{0}_{2\times3} & \boldsymbol{B}_\mathrm{t} \end{bmatrix}, \qquad (6)$$

where $\boldsymbol{0}_{i\times j}$ and $\boldsymbol{I}_{i\times j}$ represent zero and identity matrices of size (i, j), respectively. The submatrices $\boldsymbol{B}_\chi$, $\boldsymbol{B}_{\mathrm{c},\chi}$, $\boldsymbol{B}_{\mathrm{d},\chi}$, $\boldsymbol{B}_{\mathrm{s},\chi}$, and $\boldsymbol{B}_{\mathrm{t},\chi}$ represent the internal interconnection structure of the network vertices and their connections to converters, subsystems, sources, and sinks in the electricity and gas domain $\chi \in \{\mathrm{e}, \mathrm{g}\}$. The submatrix $\boldsymbol{B}_\mathrm{c}$ describes the relation between the converter vertex and edges. The submatrix $\boldsymbol{B}_{\mathrm{s,d}}$ represents the influence of the ambient atmosphere on subsystems. The submatrix $\boldsymbol{B}_\mathrm{t}$ describes the relation between the sink vertices and the corresponding edges. Vertices $v \in \mathcal{V}_\mathrm{e}$ and $v \in \mathcal{V}_\mathrm{g}$ represent voltage and pressure nodes, respectively, which corresponds to effort nodes in the generalized framework. Flows over the edges $a \in \mathcal{E}_\mathrm{e} \cup \mathcal{E}_{\mathrm{d,e}} \cup \mathcal{E}_{\mathrm{s,e}} \cup \mathcal{E}_{\mathrm{t,e}}$ and $a \in \mathcal{E}_\mathrm{g} \cup \mathcal{E}_{\mathrm{d,g}} \cup \mathcal{E}_{\mathrm{s,g}} \cup \mathcal{E}_{\mathrm{t,g}}$ specify currents and volume flows, respectively, which corresponds to flows in the generalized framework.

3.2 Subsystem Modeling

Electrical Line The set $\mathcal{E}_\mathrm{e}$ represents three-phase lines in the electrical network. As our model focuses on dynamic processes with time constants $T \geq 1\,\mathrm{s}$, the electrical network can be assumed to be in steady state, which leads to a phasor representation of the network variables (Dörfler and Bullo, 2012). The three-phase system of lines is modeled by considering the single-phase equivalent (Schiffer et al., 2016), where a single-phase line segment is described by a π-section equivalent circuit (Fiaz et al., 2013) with its phasor bond graph (Núñez Hernández et al., 2014) depicted in Fig. 4(a). The generalized variables are two-dimensional phasors, which contain the real and imaginary parts of the complex voltages and currents they represent. At MV level, the π-section equivalent circuit can

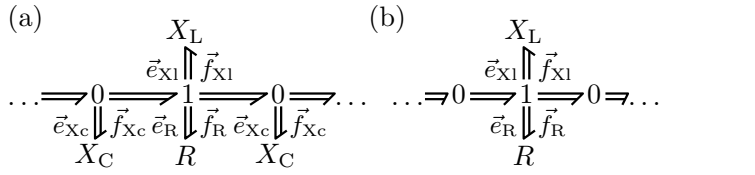

Fig. 4. Phasor bond graphs of a π-section equivalent circuit (a) and an ohmic-inductive line (b)

further be simplified by neglecting the shunt parameters (Heuck et al., 2010, pp. 238–239). Hence, electrical lines are modeled by an ohmic-inductive, single-phase equivalent circuit. Its corresponding phasor bond graph is illustrated in Fig. 4(b). The constitutive equations for the impedances are given by (Núñez Hernández et al., 2014)

$$\begin{bmatrix} \Re\{\vec{e}_{\mathrm{R}i}\} \\ \Im\{\vec{e}_{\mathrm{R}i}\} \end{bmatrix} = R_i \begin{bmatrix} 1 & 0 \\ 0 & 1 \end{bmatrix} \begin{bmatrix} \Re\{\vec{f}_{\mathrm{R}i}\} \\ \Im\{\vec{f}_{\mathrm{R}i}\} \end{bmatrix}, \qquad i \in \mathcal{E}_\mathrm{e}, \qquad (7)$$

$$\begin{bmatrix} \Re\{\vec{e}_{\mathrm{X}i}\} \\ \Im\{\vec{e}_{\mathrm{X}i}\} \end{bmatrix} = X_i \begin{bmatrix} 0 & -1 \\ 1 & 0 \end{bmatrix} \begin{bmatrix} \Re\{\vec{f}_{\mathrm{X}i}\} \\ \Im\{\vec{f}_{\mathrm{X}i}\} \end{bmatrix}, \qquad i \in \mathcal{E}_\mathrm{e}. \qquad (8)$$

Gas Pipe Pressure is the essential operational variable in gas networks. Pipe models usually focus on wall friction effects which cause pressure drops over the length of a pipe. These pressure losses are commonly calculated by the *Darcy-Weißbach equation* (Cerbe, 2004, p. 123) that results from the conservation of momentum under the following idealization assumptions congregated from Cerbe (2004), Lurie (2008), and Rüdiger (2009):

(1) One-dimensional flow in x direction
(2) Constant pipe parameters A, d, l, and k
(3) All variables specifying the gas flow are average values over the cross-sectional area A
(4) Independence of ambient temperature T due to underground placement of pipes at distribution level
(5) Calculation of λ limited to turbulent flows (Zanke's equation)
(6) Inner friction in the gas is neglected
(7) Stationary gas flow
(8) Incompressible gas (hence, mass flow conservation simplifies to volume flow conservation)

(9) Besides wall friction, no other effects that cause pressure differences between the start and end of a pipe (e.g. elevation profile) are considered

It establishes a nonlinear, resistive relation for the pressure losses induced by a volume flow through a pipe

$$\Delta p_{\mathrm{R}} = \operatorname{sgn}(Q) \cdot \frac{\lambda(Q) \cdot \varrho \cdot l}{2 \cdot d \cdot A^2} \cdot Q^2 \tag{9}$$

with volume flow $Q = v \cdot A$, gas density ϱ, pipe length l, pipe diameter d, and cross-sectional area A. The dimensionless pipe friction factor $\lambda(Q)$, which is essential for the consideration of friction pressure losses, is calculated by the explicit equation after Zanke (Cerbe, 2004, p. 124). As a result, the pipes can be modeled as shown in the GBG in Fig. 3. According to (9), the constitutive equations of the resistive elements are given by

$$e_{\mathrm{R}j} = R_j(f_{\mathrm{R}j}) f_{\mathrm{R}j}^2, \quad j \in \mathcal{E}_{\mathrm{g}}. \tag{10}$$

Network Vertices The vertices in the electrical network $v \in \mathcal{V}_{\mathrm{e}}$ and in the gas network $v \in \mathcal{V}_{\mathrm{g}}$ are modeled as lossless effort nodes, which are subject to Kirchoff's current law. Hence, they are described by a *0-junction*.

Environmental Interaction The MEDS in Fig. 1 is subject to multiple interactions with its system environment. From a PHS point of view, these interactions are part of the interaction port $\mathcal{I}$. Firstly, the electrical and gas networks are connected to superordinate networks. As the voltages and pressures at higher system levels are only slightly affected by the MEDS, the superordinate networks can be modeled as ideal effort sources. Secondly, the transformer substations and gas pressure-regulating stations are connected to subordinate networks. Fiaz et al. (2013) model the subordinate networks as resistive elements. However, in MEDSs the demand of these networks is highly volatile and cannot be modeled by a constant resistor. Instead, the subordinate networks are modeled as ideal flow sources. Thirdly, the MEDS is subject to interaction with its ambient atmosphere. Regarding the exemplary MEDS, wind power induces a mechanical torque on the rotor blades of the wind turbine. Hence, the wind power interaction is modeled by an ideal flow source.

Power-to-gas Unit Vertex $v \in \mathcal{V}_{\mathrm{C}} = \{14\}$ represents the P2G unit which transforms electrical energy to synthetic gas through a complex process comprising electrolysis and methanization. Since this process has to be controlled, the subsystem P2G unit represents a closed-loop system. However, the original application of the PHS approach is the modeling of open-loop systems and their subsequent control on the basis of the open-loop model. Hence, the representation of already closed-loop systems within the PHS framework poses a non-trivial challenge. We address this issue by considering the P2G unit as modulated transformer with time-varying transformation factor $\alpha(t)$ to model controlled behavior. All conversion losses are summarized on electrical DC side by a single series resistance. Furthermore, the P2G unit is assumed to consume purely active power, i.e. the phasors $\vec{I}_{13}$ and $\vec{U}_1$ that specify the power infeed into the P2G unit are in phase. Since $\vec{U}_1 = U_1 = e_{13}$ is set as reference voltage for the electrical network, $\vec{I}_{13} = I_{13} = f_{13}$. Thus, the P2G connection to the electrical network can be modeled as single bond instead of a phasor bond. The resulting GBG is illustrated in Fig. 5. The resistor is specified by Ohm's

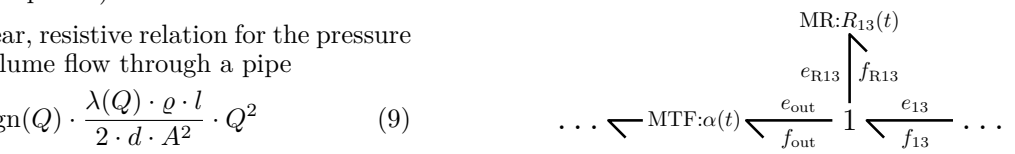

Fig. 5. GBG of the P2G unit

law $e_{\mathrm{R13}} = R_{13} \cdot f_{\mathrm{R13}}$ with

$$R_{13}(t) = \frac{e_{13}(t)}{f_{13}(t)} \cdot (1 - \eta). \tag{11}$$

The resistance (11) is obtained from the power balance

$$P_{\mathrm{out}} = \eta P_{13} = P_{13} - P_{\mathrm{R}}, \tag{12}$$

$$\eta e_{13} f_{13} = e_{13} f_{13} - e_{\mathrm{R13}} f_{\mathrm{R13}}. \tag{13}$$

Insertion of $e_{\mathrm{R13}} = R_{13} \cdot f_{\mathrm{R13}}$ and $f_{\mathrm{R13}} = f_{13}$ yields

$$\eta e_{13} = e_{13} - R_{13} f_{13}, \tag{14}$$

which can easily be transformed into (11).

Wind Turbine A wind turbine is a complex dynamic system which contains numerous control loops. Hackl et al. (2015) developed a high-order dynamic model of variable-speed synchronous generator wind turbines for the relation between the incoming wind speed and the produced power output. The model includes dynamic processes down to a time scale of microseconds. As the MEDS model of our publication aims at time constants $T \geq 1\,\mathrm{s}$, the model of Hackl et al. (2015) is simplified by making the following assumptions:

(1) The dynamics are reduced to the rotor inertia and the DC link capacitor. Electrical losses are neglected.
(2) The current $I_{\mathrm{W}} = f_{16}$ fed into the network is taken as control variable ($\Im\{I_{\mathrm{W}}\} = 0$). The issue of modeling the closed-loop behavior caused by the generator current controller is addressed similarly to the P2G unit by a time-varying conversion factor $\beta(t)$.

By these assumptions, a second-order explicit PHS model of the wind turbine can be formulated as

$$\begin{bmatrix} \dot{x}_1 \\ \dot{x}_2 \end{bmatrix} = \underbrace{\begin{bmatrix} 0 & -\frac{1}{\beta(t)} \\ \frac{1}{\beta(t)} & 0 \end{bmatrix}}_{\boldsymbol{J}} \frac{\partial H_{\mathrm{W}}}{\partial \boldsymbol{x}} + \begin{bmatrix} 0 \\ 1 \end{bmatrix} u + \begin{bmatrix} 1 \\ 0 \end{bmatrix} d, \tag{15}$$

$$\begin{bmatrix} z \\ y \end{bmatrix} = \begin{bmatrix} 1 & 0 \\ 0 & 1 \end{bmatrix} \frac{\partial H_{\mathrm{W}}}{\partial \boldsymbol{x}}, \tag{16}$$

$$H_{\mathrm{W}} = \tfrac{1}{2J} x_1^2 + \tfrac{1}{2C} x_2^2. \tag{17}$$

The two energy states are given by the angular momentum of the wind turbine rotor $x_1 = L$ and the charge of the DC link capacitor $x_2 = Q$. For convenience and in consideration of the phasor network modeling, the controllable input $u = I_{\mathrm{W}}$ is set to the real part of the phasor $\vec{f}_{16}$ with $\Im\{\vec{f}_{16}\} = 0$. The uncontrollable input is the wind-induced torque $d = M_{\mathrm{wind}} = f_{\mathrm{wind}}$ that acts on the rotor. The corresponding controllable and uncontrollable outputs are given by $y = \Re\{\vec{e}_{16}\}$ and $z = e_{\mathrm{wind}}$. The parameters J and C are the turbine's inertia and the capacitance of the DC link capacitor, respectively.

Energy storages Similar to the P2G unit, the energy storages $v \in \{15, 17\}$ are closed-loop systems whose detailed modeling is outside the scope of this publication. Generally, energy storage in the GBG framework is represented as C-type storage element described by an energy state x. However, in the present closed-loop case, the relation between e and x cannot simply be expressed by a constant C. This issue is addressed by considering the energy storages as flow sources. The stored energy of the storage systems can then be calculated as

$$E = -3 \cdot \int \Re\{\vec{e}_{15} \cdot \vec{f}_{15}^{*}\}\,\mathrm{d}t - \int e_{17} \cdot f_{17}\,\mathrm{d}t, \tag{18}$$

where the factor 3 stems from the three-phase nature of the electrical system.

3.3 Overall Model

The modeling process is concluded by reassembling the GBGs of the separately modeled subsystems into the GBG in Fig. 3. The gray bonds indicate the three-phase nature of the electrical system. Note that the constitutive equations for the pipe resistances are nonlinear. Thus, the PHS derived from this GBG cannot be given in standard input-state-output form but results in an *implicit* formulation (van der Schaft and Jeltsema, 2014, p. 53).

Dirac Structure From the generalized junction structure of the GBG (circled in gray in Fig. 3), it is straightforward to obtain the Dirac structure without the explicit wind turbine PHS. It is specified by $\widetilde{\boldsymbol{F}}\widetilde{\boldsymbol{f}} + \widetilde{\boldsymbol{E}}\widetilde{\boldsymbol{e}} = \boldsymbol{0}$ with 1×43 vectors $\widetilde{\boldsymbol{e}} = [\,\boldsymbol{e}_\mathrm{e}\ \boldsymbol{e}_\mathrm{g}\,]^\mathsf{T}$, and $\widetilde{\boldsymbol{f}} = [\,\boldsymbol{f}_\mathrm{e}\ \boldsymbol{f}_\mathrm{g}\,]^\mathsf{T}$, where the first 13 elements are two-dimensional phasors

$$\boldsymbol{e}_\mathrm{e} = [\,\vec{e}_{\mathrm{R}i}\ \vec{e}_{\mathrm{X}i}\ \vec{e}_{15}\ \vec{e}_{16}\ \vec{e}_{18}\ \vec{e}_{21}\ \ldots\ \vec{e}_{24}\,]^\mathsf{T}, \quad i \in \mathcal{E}_\mathrm{e}, \tag{19}$$

$$\boldsymbol{f}_\mathrm{e} = [\,\vec{f}_{\mathrm{R}i}\ \vec{f}_{\mathrm{X}i}\ \vec{f}_{15}\ \vec{f}_{16}\ \vec{f}_{18}\ -\vec{f}_{21}\ \ldots\ -\vec{f}_{24}\,]^\mathsf{T}, \tag{20}$$

and the remaining 17 elements are the generalized variables

$$\boldsymbol{e}_\mathrm{g} = [\,e_{\mathrm{R}j}\ e_{14}\ e_{17}\ e_{19}\ e_{25}\ \ldots\ e_{29}\,]^\mathsf{T}, \quad j \in \mathcal{E}_\mathrm{g}, \tag{21}$$

$$\boldsymbol{f}_\mathrm{g} = [\,f_{\mathrm{R}j}\ f_{14}\ f_{17}\ f_{19}\ -f_{25}\ \ldots\ -f_{29}\,]^\mathsf{T}, \tag{22}$$

of the P2G unit and the gas domain (see Fig. 3). The matrices $\widetilde{\boldsymbol{F}}$ and $\widetilde{\boldsymbol{E}}$ are of corresponding size 43×43 and cannot be given explicitly for reasons of space. They simply represent the 0-/1-junction, and MTF equations which correlate the generalized variables $\widetilde{\boldsymbol{e}}$ and $\widetilde{\boldsymbol{f}}$. Hence, they contain entries inside the set $\{0, \pm 1, \alpha(t)\}$.

Implicit Port-Hamiltonian System Model The implicit PHS model of the MEDS is given by

$$\widetilde{\boldsymbol{F}}\widetilde{\boldsymbol{f}} + \widetilde{\boldsymbol{E}}\widetilde{\boldsymbol{e}} = \boldsymbol{0}, \tag{23}$$

$$\begin{bmatrix}\Re\{\vec{e}_{\mathrm{R}i}\}\\ \Im\{\vec{e}_{\mathrm{R}i}\}\end{bmatrix} = R_i \begin{bmatrix}1 & 0\\ 0 & 1\end{bmatrix} \begin{bmatrix}\Re\{\vec{f}_{\mathrm{R}i}\}\\ \Im\{\vec{f}_{\mathrm{R}i}\}\end{bmatrix}, \tag{24}$$

$$\begin{bmatrix}\Re\{\vec{e}_{\mathrm{X}i}\}\\ \Im\{\vec{e}_{\mathrm{X}i}\}\end{bmatrix} = X_i \begin{bmatrix}0 & -1\\ 1 & 0\end{bmatrix} \begin{bmatrix}\Re\{\vec{f}_{\mathrm{X}i}\}\\ \Im\{\vec{f}_{\mathrm{X}i}\}\end{bmatrix}, \tag{25}$$

$$e_{\mathrm{R}j} = R_j(f_{\mathrm{R}j}) f_{\mathrm{R}j}^2, \tag{26}$$

$$H(\boldsymbol{x}) = H_\mathrm{W}(\boldsymbol{x}) = \tfrac{1}{2J} x_1^2 + \tfrac{1}{2C} x_2^2, \tag{27}$$

$$\begin{bmatrix}\dot{x}_1\\ \dot{x}_2\\ e_\mathrm{wind}\\ \Re\{\vec{e}_{16}\}\end{bmatrix} = \begin{bmatrix}\boldsymbol{J}_{2\times2}\\ \boldsymbol{I}_{2\times2}\end{bmatrix} \frac{\partial H}{\partial \boldsymbol{x}} + \begin{bmatrix}\boldsymbol{I}_{2\times2}\\ \boldsymbol{0}_{2\times2}\end{bmatrix} \begin{bmatrix}f_\mathrm{wind}\\ -\Re\{\vec{f}_{16}\}\end{bmatrix}, \tag{28}$$

with $i \in \mathcal{E}_\mathrm{e}$ and $j \in \mathcal{E}_\mathrm{g}$, where (24) and (25) are the constitutive equations for the line impedances, (26) are the nonlinear, constitutive equations for the pipe resistances and (27) is the Hamiltonian that represents the stored energy in the wind turbine. The total stored energy within the MEDS is given by

$$E = H(\boldsymbol{x}) - 3 \cdot \int \Re\{\vec{e}_{15} \cdot \vec{f}_{15}^{*}\}\,\mathrm{d}t - \int e_{17} \cdot f_{17}\,\mathrm{d}t. \tag{29}$$

Equations (23) and (28) can be transformed to (2) by

$$\begin{bmatrix}\boldsymbol{I}_{2\times2}\\ \boldsymbol{0}_{45\times2}\end{bmatrix} \begin{bmatrix}\dot{x}_1\\ \dot{x}_2\end{bmatrix} = \begin{bmatrix}\boldsymbol{J}_{2\times2}\\ -\boldsymbol{I}_{2\times2}\\ \boldsymbol{0}_{43\times2}\end{bmatrix} \frac{\partial H}{\partial \boldsymbol{x}} + \left[\begin{array}{c|cc|c} 1 & \multicolumn{2}{c|}{\multirow{2}{*}{$\boldsymbol{0}_{2\times6}$}} & 0 & \multirow{2}{*}{$\boldsymbol{0}_{2\times36}$}\\ 0 & & & -1 & \\ \hline \vdots & \multicolumn{4}{c}{\multirow{2}{*}{$\boldsymbol{0}_{2\times43}$}}\\ \hline 0 & \multicolumn{4}{c}{} \end{array}\right] \begin{bmatrix}f_\mathrm{wind}\\ \widetilde{\boldsymbol{f}}\end{bmatrix}$$

$$+ \left[\begin{array}{c|cc|c} \multicolumn{5}{c}{$\boldsymbol{0}_{2\times44}$}\\ \hline 1 & \multicolumn{2}{c|}{\multirow{2}{*}{$\boldsymbol{0}_{2\times6}$}} & 0 & \multirow{2}{*}{$\boldsymbol{0}_{2\times36}$}\\ 0 & & & 1 & \\ \hline \boldsymbol{0}_{43\times1} & \multicolumn{4}{c}{$\widetilde{\boldsymbol{E}}_{43\times43}$} \end{array}\right] \begin{bmatrix}e_\mathrm{wind}\\ \widetilde{\boldsymbol{e}}\end{bmatrix}. \tag{30}$$

All remaining, unspecified elements are either effort or flow sources. Their constitutive equations are time series for the efforts e_j with $j \in \mathcal{V}_\mathrm{s}$ and flows f_j with $j \in \mathcal{E}_\mathrm{t} \cup \{15, 17\}$. Note that (30) is a DAE system (cf. Beattie et al. (2017)).

4. SIMULATION

In order to assess the plausibility of the obtained implicit PHS model, it is implemented in *OpenModelica* and simulated by using the *dassl* solver with default parameters. The simulation is performed on the basis of real measurements provided by a distribution system operator and data obtained from the gas network analysis tool STANET. As the closed-loop behavior of the MEDS shall be evaluated, the control signals and parameters need to be specified. For the wind turbine, a maximum point power tracking generator control and a PI controller for the DC link is implemented (Hackl et al., 2015, p. 1608). For the electrical storage, gas storage, and P2G unit, heuristic control schemes are applied. For reasons of space it is not possible to present the simulation inputs at this point. Instead, the complete set of parameters is provided on `https://www.irs.kit.edu/mathmod18.php`. The data feature a winter scenario with significant wind velocities and thus prevailing wind power infeed at vertex 4. This causes reversed power flow from vertex 4 to vertex 1, and from there into the HV level. In the gas distribution system, a high gas consumption with volume flows up to $0.25\,\mathrm{m}^3/\mathrm{s}$ is represented.

In Fig. 6, the magnitude of the measured voltage U_1, which serves as a simulation input, is depicted in gray. In addition, the magnitude of the simulated voltage U_4 is illustrated in black. It is evident that the magnitude of U_4 is higher than the magnitude of U_1, which corresponds to the expected behavior caused by the wind power infeed at vertex 4. As there are more measurements than simulation inputs, the simulated magnitude of U_4 can be compared with the measured magnitude U_4, which is not part of the simulation. By this comparison an average error of $-58.53\,\mathrm{V}$ is obtained. Referred to nominal voltage of 20 kV, the corresponding average relative error is $-0.293\,\%$. In Fig. 7, three simulated vertex pressures in the gas distribution system are illustrated. It is observed that the pressure

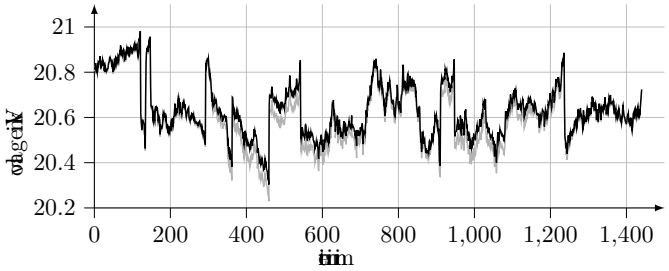

Fig. 6. Magnitudes of measured voltage U_1 (gray) and simulated voltage U_4 (black)

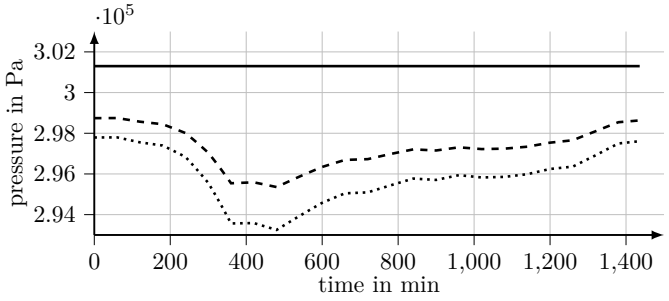

Fig. 7. Simulated pressures at vertices 5,8,13 (solid, dashed, dotted)

decreases the further the pressure nodes are away from the pressure control station at vertex 5. Due to the modeled friction effects this behavior is plausible. In the course of the simulated scenario, the deviation of the simulated pressures from the provided STANET data remains below 140 Pa. Referred to nominal gauge pressure of 3 bar this corresponds to a relative error of less than 0.05 %.

5. CONCLUSION

PHSs represent a consistent approach for the control-oriented modeling of MEDSs. Due to the modularity of PHSs, subsystems can be modeled individually and afterwards be integrated in an overall system model. Resulting from a nonlinear resistive relation, the PHS cannot be formulated in the standard input-state-output form (van der Schaft and Jeltsema, 2014, p. 53). Instead, an implicit differential-algebraic PHS can be obtained. The modeling of closed-loop subsystems proved to be challenging. Future work will address this issue and generalize the case study of this publication to the modeling of arbitrary MEDSs.

REFERENCES

Arnold, M., Negenborn, R.R., Andersson, G., and De Schutter, B. (2009). Model-based predictive control applied to multi-carrier energy systems. In *Proc. IEEE PES Gen. Meet, 2009*, 1–8.

Beattie, C., Mehrmann, V., Xu, H., and Zwart, H. (2017). Port-hamiltonian descriptor systems. *arXiv preprint arXiv:1705.09081*.

Cerbe, G. (2004). *Grundlagen der Gastechnik: Gasbeschaffung, Gasverteilung, Gasverwendung*. Carl Hanser Verlag, München Wien, 6 edition.

de Durana, J.M.G., Barambones, O., Kremers, E., and Varga, L. (2014). Agent based modeling of energy networks. *Ener. Conv. Manage.*, 82, 308–319.

Dörfler, F. and Bullo, F. (2012). Synchronization and transient stability in power networks and nonuniform kuramoto oscillators. *SIAM J. Control Optim.*, 50(3), 1616–1642.

Duindam, V., Macchelli, A., Stramigioli, S., and Bruyninckx, H. (2009). *Modeling and Control of Complex Physical Systems*. Springer-Verlag, Berlin Heidelberg.

Fiaz, S., Zonetti, D., Ortega, R., Scherpen, J.M., and van der Schaft, A. (2013). A port-hamiltonian approach to power network modeling and analysis. *Eur. J. Control*, 19(6), 477–485.

Geidl, M. and Andersson, G. (2005). A modeling and optimization approach for multiple energy carrier power flow. In *2005 IEEE Power Tech*, 1–7. IEEE.

Hackl, C.M., Dirscherl, C., and Schechner, K. (2015). Modellierung und Regelung von Windkraftanlagen. In D. Schröder (ed.), *Elektrische Antriebe – Regelung von Antriebssystemen*, 1540–1613. Springer, Berlin.

Heuck, K., Dettmann, K.D., and Schulz, D. (2010). *Elektrische Energieversorgung*. Vieweg+Teubner, Wiesbaden.

Hohmann, S., Maaß, H., Mieth, C., Pfeifer, M., Wagner, D., and Wegner, F. (2017). Graph-theoretic model for observability in multi-carrier energy distribution networks. *Computer Science-Research and Development*.

Jansen, L. and Tischendorf, C. (2014). A Unified (P)DAE Modeling Approach for Flow Networks. In *Progress in Differential-Algebraic Equations*, Differential-Algebraic Equations Forum, 127–151. Springer.

Lurie, M. (2008). *Modeling of oil product and gas pipeline transportation*. Wiley-VCH, Weinheim.

Mancarella, P. (2014). MES (multi-energy systems): An overview of concepts and evaluation models. *Energy*, 65, 1–17.

Martinez-Mares, A. and Fuerte-Esquivel, C.R. (2012). A unified gas and power flow analysis in natural gas and electricity coupled networks. *IEEE Trans. Power Syst.*, 27(4), 2156–2166.

Núñez Hernández, I., Breedveld, P.C., Weustink, P.B., and Gonzalez-Avalos, G. (2014). Analysis of electrical networks using phasors: a bond graph approach. *International Journal of Electrical, Robotics, Electronics and Communications Engineering*, 8(7), 931–937.

Rehtanz, C. (2014). Energie- und Informationsnetze. *Automatisierungstechnik*, 62(5), 313–314.

Rüdiger, J. (2009). *Gasnetzsimulation durch Potentialanalyse*. Dissertation, Helmut-Schmidt-Universität/Universität der Bundeswehr Hamburg.

Schiffer, J., Daniele, Z., Ortega, R., Stankovic, A., Sezi, T., and Raisch, J. (2016). A survey on modeling of microgrids — from fundamental physics to phasors and voltage sources. *Automatica*, 74, 135–150.

Schulze, M. and Del Granado, P.C. (2010). Optimization modeling in energy storage applied to a multi-carrier system. In *Proc. IEEE PES Gen. Meet, 2010*, 1–7.

Sirvent, M., Kanelakis, N., Geißler, B., and Biskas, P. (2017). Linearized model for optimization of coupled electricity and natural gas systems. *J. Mod. Power Syst. Clean Energy*, 5(3), 364–374.

van der Schaft, A. and Jeltsema, D. (2014). Port-hamiltonian systems theory: An introductory overview. *Foundations and Trends® in Systems and Control*, 1(2-3), 173–378.